FELDER, S., and CHANSON, H. (2014). "Air–water Flows and Free-surface Profiles on a Non-uniform Stepped Chute." *Journal of Hydraulic Research*, IAHR, Vol. 52, No. 2, pp. 253-263 (DOI: 10.1080/00221686.2013.841780) (ISSN 0022-1686). {http://dx.doi.org/10.1080/00221686.2013.841780}

Air-water flows and free-surface profiles on a non-uniform stepped chute

STEFAN FELDER, School of Civil Engineering, The University of Queensland, Brisbane, QLD 4072, Australia

stefan.felder@uqconnect.edu.au (Corresponding Author)

HUBERT CHANSON, (IAHR Member), School of Civil Engineering, The University of Queensland, Brisbane, QLD 4072, Australia

h.chanson@uq.edu.au

ABSTRACT

Comparative experiments were conducted between uniform and non-uniform stepped spillway profiles in a large-size laboratory facility. For each stepped configuration, the air concentration distributions matched the advective diffusion equation and the interfacial velocity was well correlated with a power law. A comparison of the air-water flow properties showed small differences in terms of number of entrained air bubbles, chord sizes and turbulence characteristics between the different configurations. For the non-uniform steps, larger flow instabilities and stronger variation in the air-water flow properties were observed. Further some non-intrusive measurements were performed with acoustic displacement meters to characterise the free-surface profiles, free-surface fluctuations and free-surface wave celerity in both non-aerated and aerated flow regions. The experiments highlighted a close agreement between experimental data and theoretical predictions in the non-aerated flows and with conductivity probe data in the aerated flows. The non-intrusive technique was suitable for measuring the free-surface characteristics on stepped chutes, especially in the non-aerated flow region.

Keywords: air-water flow, free-surface profiles, non-uniform steps, physical modelling, stepped spillways, turbulence.

1 Introduction

Stepped spillways are commonly used as flood release structures of embankment dams (Chanson 2001). The steps act as rough elements that increase the energy dissipation rates and the aeration performance compared to smooth spillways. In the last decades, several experimental studies of the air-water flows were conducted to quantify the energy dissipation performances and to provide design guidelines for flat uniform stepped spillways (e.g. Chanson 2001, Matos 2000, Boes and Hager 2003, Ohtsu *et al.* 2004, Gonzalez and Chanson 2007a). Stephenson (1988) reported an increasing energy dissipation rate on a non-uniform stepped spillway. However, detailed air-water flow measurements by Felder and Chanson (2011) on stepped spillways with

non-uniform step heights showed no increased energy dissipation rate. Despite the practical findings, the air-water flows on the non-uniform stepped spillways were not detailed. Herein the present study investigated the complex two-phase flow properties on a non-uniform stepped chute including the flow aeration, the velocity and the turbulence characteristics.

Non-uniform stepped configurations are affected by flow instabilities including jet flows and air-water surface shock waves (Toombes and Chanson 2008, Felder and Chanson 2011). Research on uniform stepped chutes provided some information about the free-surface in the clear water flow region upstream of the inception point of free-surface aeration (e.g. Amador et al. 2006, Meireles and Matos 2009, Hunt and Kadavy 2010). In the aerated flow regions, the free-surface profiles and fluctuations were rarely studied, but for the experiments with acoustic displacement meter and high-speed camera by Bung (2011,2013). In the present study, novel non-intrusive experiments were conducted with an array of acoustic displacement meters to measure the free-surface profiles, free-surface fluctuations, free-surface correlation time scales and free-surface wave celerity in both non-aerated and aerated flow regions of the non-uniform stepped spillway.

2 Experimental facility and instrumentation

2.1 Physical model

Physical experiments were conducted on a large size stepped spillway model with a large upstream stilling basin followed by a stepped spillway test section with width W = 1 m and slope θ = 26.6º. The inflow was provided through a sidewall convergent with contraction ratio 4.8:1 and a broad-crested weir with length of 0.62 m. The stepped chute section was made of plywood and the sidewalls consisted of perspex. The same stepped spillway facility was previously used in several studies with slopes of θ = 21.8º (e.g. Chanson and Toombes 2002, Chanson and Carosi 2007, Felder and Chanson 2009) and θ = 15.9º (e.g. Gonzalez and Chanson 2004). In the present study, the 26.6 º slope stepped section consisted of two configurations: i.e. 10 uniform flat steps of height h = 10 cm and a non-uniform set-up with regular alternation of two smaller size steps (h = 5 cm) and one step of h = 10 cm (Fig. 1). Figure 1 sketches the uniform and non-uniform stepped chutes including the step numbering and measurement positions at the step edges and in between the large steps for the non-uniform stepped chute.

2.2 Instrumentation

The flow discharge was deduced from a pointer gauge measurement upstream of the broad-crested weir, using the discharge calibration of Gonzalez and Chanson (2007b). The flow patterns were documented with a Canon^{TM} EOS450D dSLR camera. For both stepped configurations, detailed air-water flow experiments were conducted with phase-detection intrusive probes for transition and skimming flow discharges. A double-tip conductivity probe ($Ø$ = 0.25 mm) with transverse and longitudinal sensor distances of Δz = 2.1 mm and Δx = 7.2 mm respectively was used to measure the air-water flows at all step edges downstream of

the inception point of free-surface aeration. On the non-uniform stepped chute, experiments were also conducted half way between the large step edges. For a skimming flow rate, additional experiments were conducted with an array of two identical single-tip conductivity probes ($Ø$ = 0.35 mm) with Δx = 0 mm and various transverse separation distances 3.3 mm $\leq \Delta z \leq$ 64.1 mm at several consecutive step edges. All air-water measurements were sampled for 45 s and 20 kHz per sensor. The relative accuracy of the air-water flow measurements was about $\Delta C/C \approx 4\%$ for the void fraction C and about $\Delta V/V \approx 5\%$ for the interfacial velocity V.

Further experiments were performed in both non-aerated and aerated flow regions on the non-uniform stepped chute with an array of four acoustic displacement meters Microsonic™ aligned along the channel centreline, three Mic+25/IU/TC with 0.18 mm accuracy and 50 ms response time and one Mic+35/IU/TC sensor with 0.18 mm accuracy and 70 ms response time. The same acoustic displacement meters were used previously to measure the free-surface fluctuations in air-water flows in a hydraulic jump (e.g. Murzyn and Chanson 2009). The displacement meters were positioned perpendicular to the pseudo-bottom in channel centreline and separated with identical streamwise distance $x_j - x_i$ = 11 cm (Fig. 2b), where subscripts i and j are indices of the displacement meters. The sensors were mounted above the step edges with a distance of about 25 cm enabling a constant angle of beam spread of about 1-2 cm in radius independent of the flow depth. The sensors enabled a recording of the free-surface fluctuations at all step edges and half-way along the step cavities with h = 10 cm. It was carefully checked that no interference existed between the acoustic displacement sensors as well as with other electrical devices. The acoustic displacement meters were sampled simultaneously at 100 Hz for 300 s per sensor without any filtering. In the non-aerated flow region, some erroneous data were recorded when the free-surface was not perpendicular to the sensor beam and when the acoustic signal was not reflected accurately. A larger amount of erroneous data was recorded in the aerated flow region because of the undetermined free-surface. The strong splashing of ejected water droplets impacted sometimes directly on the sensor and manual wiping of the sensor was necessary. The recorded raw data were filtered and the erroneous points were removed. The filtering was based upon a 90% threshold of the largest and lowest raw voltage signals for the recorded 300 s signal for each sensor. The sampling duration of 300 s allowed a sufficient number of data points for all measurement positions and the advanced signal processing of the raw data.

2.3 Signal processing

The air-water flow data recorded with the double-tip conductivity probe were processed with a single-threshold technique and statistical analyses yielded the void fraction, bubble count rate, particle chord sizes, interfacial velocity and turbulence intensity. Further turbulence properties were calculated based upon the experiments with the array of two single-tip conductivity probes. For all experiments, the integral turbulent length and time scales L_{xz} and T_{int} were calculated following Chanson and Carosi (2007):

$$L_{xz} = \int_{z=0}^{z=z((R_{xz})_{max}=0)} (R_{xz})_{max} \, dz \quad (1)$$

$$T_{int} = \frac{\int_{z=0} (R_{xz})_{max} \, T_{xz} \, dz}{L_{xz}} \quad (2)$$

where $(R_{xz})_{max}$ is the maximum cross-correlation coefficient between the two single-tip probes and T_{xz} is the transverse cross-correlation time scale integrated from the maximum of the cross-correlation function to the first crossing. The integral turbulent length scale L_{xz} represents a characteristic transverse length of the large vortical structures advecting the air-water packets (Chanson and Carosi 2007) and T_{int} is the corresponding time scale.

The statistics of the acoustic displacement meter signals were analysed, thus giving some information about the free-surface profiles, free-surface fluctuations and free-surface time scales as well as the free-surface wave celerity.

2.4 Experimental flow conditions

In free-surface flows, the physical modelling is commonly based upon a Froude similitude and the present study is no exception. Experiments were conducted for a wide range of discharges per unit width q_w between 0.005 m^2/s and 0.241 m^2/s corresponding to a dimensionless discharge d_c/h between 0.13 and 1.81 where d_c is the critical flow depth. The flow rates corresponded to Reynolds numbers defined in terms of the hydraulic diameter between 1.9×10^4 and 9.6×10^5 (Table 1). The measurements with the conductivity probes were conducted in the transition and skimming flow regimes for flow rates in the range from 0.056 m^2/s to 0.227 m^2/s. On the non-uniform stepped chute, the experiments with the acoustic displacement meters comprised several flow rates between 0.075 m^2/s and 0.202 m^2/s. Table 1 summarises the experimental program for the conductivity probe and acoustic displacement sensor experiments on the non-uniform stepped spillway and for the reference configuration with uniform step height. More details about the experimental facility, the instrumentation and signal processing can be found in Felder (2013).

3 Air-water flow patterns

The flow above the uniform stepped spillway showed typical flow patterns with characteristic features of nappe, transition and skimming flow regimes. For the smallest flow rates, corresponding to $d_c/h < 0.59$, the flow pattern consisted of free-falling nappes typical for embankment dam stepped spillways (Toombes 2002). For intermediate discharges, the air-water transition flows showed small instabilities resulting in strong droplet splashing downstream of the inception point of air entrainment. The observations were consistent with the findings by Chanson and Toombes (2004). For discharges such as $d_c/h > 0.91$, the flow skimmed over the pseudo-bottom formed by the step edges exhibiting a typical skimming flow regime

(Rajaratnam 1990).

The flow patterns on the non-uniform stepped spillway showed flow features similar to those observed on the uniform stepped chute. For the nappe flow regime with $d_c/h < 0.53$, the water cascaded down the stepped spillway in free-falling nappes. The step cavities for the 5 cm high steps contained a large void and it appeared that the free-falling jets flowed from 10 cm step to 10 cm step bypassing the smaller step cavities. In the transition flow regime, strong droplet splashing was observed and the flow appeared unstable (Fig. 2a). The flow was similar to transition flows on the uniform stepped spillways, but recirculation motions were observed in the smaller step cavities. In skimming flows ($d_c/h > 0.97$), the air-water flow patterns were identical to uniform stepped spillways with the free-surface being parallel to the pseudo-bottom formed by the step edges (Fig. 2b). Note that some large scale tornado eddies were generated in the upstream corners of the broad-crested weir as observed previously by Gonzalez and Chanson (2007b). The longitudinal vortices propagated downstream and caused free-surface disturbances and fluctuations in the clear water flow region (Fig. 2b). The free-surface instabilities increased with increasing flow rate.

4 Air-water flow properties

A range of air-water flow properties was measured in the aerated flow region downstream of the inception point of free-surface aeration in transition and skimming flows. The experiments were conducted with double-tip conductivity probes at step edges in channel centreline. For the non-uniform configurations, the air-water flow properties were additionally measured in the centre of the large step cavity. Additional air-water flow properties were recorded with an array of two single-tip conductivity probes for several consecutive step edges in a skimming flow regime.

4.1 Basic air-water flow properties

The void fraction distributions on both non-uniform and uniform stepped spillways were exhibited a characteristic S-shape profile for both stepped configurations (Fig. 3). Figure 3 shows typical void fraction distributions for a skimming flow rate in dimensionless form as functions of the dimensionless distance from the pseudo-bottom y/Y_{90}, where Y_{90} is the depth with $C = 0.90$. The void fraction distributions were in relatively close agreement, but some scatter of the distribution shapes was observed for the non-uniform stepped spillway reflecting the sudden changes in step heights. In particular the void fraction distributions recorded between the 10 cm high step edges showed slightly different shapes, with larger air concentrations close to the pseudo-bottom (Fig. 3). Larger values of void fraction in between step edges were reported for uniform stepped spillways (e.g. Gonzalez and Chanson 2004) and this was not a specific feature for the non-uniform stepped spillway. The legend of Fig. 3 lists also the depth-averaged mean air concentrations C_{mean} at the measurement positions. The data showed comparatively smaller mean air concentration downstream of the large steps on the non-uniform stepped spillway. This trend was observed for all experiments, but the reason for the reduced mean air concentration remained unclear. Despite the differences, all void fraction

distributions showed a good agreement with the advective diffusion equation for air bubbles developed by Chanson and Toombes (2002):

$$C = 1 - tanh^2\left(K' - \frac{y/Y_{90}}{2\,D_o}\right) + \frac{(y/Y_{90} - 1/3)^3}{3\,D_o} \quad (3)$$

where K' is an integration constant and D_o is a function of C_{mean} only. The mean air concentration C_{mean} characterises the depth-averaged air content in terms of Y_{90}: $C_{mean} = 1 - d/Y_{90}$ where d is the equivalent clear water flow depth:

$$d = \int_0^{Y_{90}} (1 - C)\,dy \quad (4)$$

Equation (3) compared well with void fraction distributions on the non-uniform stepped chute (Fig. 3), and the finding was independent of the step height as previously reported by Felder and Chanson (2009).

For all experiments, the dimensionless distributions of bubble count rate $F\,d_c/V_c$, where V_c is the critical flow velocity, showed distinctive differences between the uniform and non-uniform stepped spillways (Fig. 4). All dimensionless distributions of $F\,d_c/V_c$ exhibited typical shapes with large bubble count rates in the intermediate flow region for $0.3 < C < 0.7$ and much smaller bubble counts in the bubbly flow ($0 < C < 0.3$) and spray regions ($1 > C > 0.7$) (Fig. 4). For the uniform stepped spillway, the bubble count rates were larger than on the non-uniform stepped chute. It appeared that the number of entrained air bubbles was reduced by the presence of smaller step heights. The observation was in agreement with some findings of scale effects in terms of bubble frequencies for geometrically scaled uniform stepped spillways (Felder and Chanson 2009), with lesser dimensionless bubble count rates observed on stepped spillways with smaller step heights.

The interfacial velocities were calculated based upon cross-correlation analyses of the raw data of the double-tip conductivity probe sensors. For both stepped spillways, the dimensionless interfacial velocities V/V_{90} were compared for all transition and skimming flow discharges as a function of y/Y_{90} (Fig. 5); where V_{90} is the characteristic interfacial velocity with $C = 0.90$. Overall the data were in very good agreement and they were close to a $1/10^{th}$ power law correlation for $y/Y_{90} \leq 1$ and a uniform profile for $y/Y_{90} > 1$:

$$\frac{V}{V_{90}} = \left(\frac{y}{Y_{90}}\right)^{1/N} \qquad y/Y_{90} \leq 1 \quad (5)$$

$$\frac{V}{V_{90}} = 1 \qquad y/Y_{90} > 1 \quad (6)$$

The agreement between all experimental data and Eqs. (5) and (6) was independent of the step heights and the measurement position along the stepped chutes (Fig. 5). Some scatter of the interfacial

velocity data in the spray region was predominantly observed for the transition flow data characterised by large droplet ejections. Furthermore, the data scatter was larger for the more unstable flow on the non-uniform stepped chute.

The integration of the correlation functions of double-tip conductivity probe signals provided information about the auto- and cross-correlation time scales, i.e. characteristic times of the longitudinal and transverse connection between the air-water structures. The correlation time scales are a longitudinal measure of the advecting vortices in the turbulent air-water flow. While the auto-correlation time scales showed a close agreement between uniform and non-uniform stepped configurations, the cross-correlation time scales for the non-uniform stepped chute showed a significant data scatter and smaller maximum time scales in the intermediate flow region. The magnitude of the auto- and cross-correlation time scales was about 0.001 s in the bubbly and spray flow regions, and the maximum time scales were about 0.01 s in the bulk of the flow. The data are not presented herein, but may be found in Felder (2013).

The chord sizes of air bubbles and water droplets were calculated to provide information on the millimetric and sub-millimetric scales (Fig. 6). Typical probability distribution functions of air bubble chord sizes are presented for a step edge, showing differences between the non-uniform and uniform stepped spillways (Fig. 6a). Some differences in terms of chord size probability distribution functions (PDF) were observed with a smaller amount of small air bubbles and a larger amount of larger chord sizes for the non-uniform stepped chute (Fig. 6a). For the same step edge, the comparison of water droplet chord sizes showed a good agreement between the non-uniform and uniform stepped spillways (Fig. 6b). On the non-uniform stepped spillway, it appeared that the spray region was not affected by the changing step heights while the air bubble chord sizes were comparatively larger in the bubbly flow region.

4.2 Turbulence characteristics

The turbulence intensity calculation in air-water flows is based upon the shape of the auto- and cross-correlation functions of the double-tip probe data (Chanson and Toombes 2002). The turbulence intensity *Tu* provided information about the velocity fluctuations within the air-water flow. The comparison of turbulence intensity distributions for the two stepped spillways showed a relatively good agreement in distribution shape for all experiments (Fig. 7). All profiles showed large turbulent levels in the intermediate flow region and smaller levels of turbulence in the bubbly flow and spray regions. The turbulence intensities were largest on the uniform stepped spillway at most step edges. On the non-uniform stepped spillway, the turbulence levels showed some data scatter, with larger turbulent levels in the bubbly flow region for the measurement positions between the 10 cm high step edges (Fig. 7). Overall the turbulence levels on the uniform stepped chute were about 20-50% larger for an identical flow rate. The presence of the smaller steps on the non-uniform stepped spillway reduced the turbulence intensities, possibly linked with wake interference at the large step. The observations were consistent with the earlier observations of comparatively larger turbulence levels on geometrically larger step heights (Felder and Chanson 2009).

Further turbulent air-water flow properties included the integral turbulent length and time scales calculated based upon the measurements with an array of two single-tip conductivity probes (Eqs. (1) and (2)). The turbulent length and time scales L_{xz} and T_{int} are a measure of the large advecting vortices in transverse direction. Overall the dimensionless distributions of both integral turbulent length and time scales showed relatively good agreement for the uniform and non-uniform stepped spillways (Fig. 8). For the turbulent length scales, the shapes of the distributions were comparable with a maximum in the intermediate flow region (Fig. 8a). For the non-uniform stepped spillway, larger scatter of distributions was observed and the length scales appeared slightly smaller. The comparative analysis of dimensionless integral turbulent time scale distributions showed some deviation of shapes for the non-uniform configuration, compared to typical observations on the uniform stepped chute (Fig. 8b). In particular the time scale distribution measured in between the step edges with h = 10 cm (dashed line) showed a different shape with some maximum values close to the pseudo-bottom (Fig. 8b). For both uniform and non-uniform stepped configurations, larger turbulent time scales were observed in the upper spray region which was linked with ejected droplets not interacting with the mainstream flow (Chanson and Carosi 2007).

For all experiments, the characteristic maximum integral turbulent length and time scales were recorded and added to the legend in Fig. 8. Overall the uniform stepped spillway flow exhibited larger maximum integral turbulent scales. For the non-uniform stepped spillway, some scatter of the maximum time and length scales was observed, suggesting that the different step heights affected the sizes of arge turbulent eddies within the two-phase flows. The present findings are in agreement with some observations of scale effects by Felder and Chanson (2009) on geometrically scaled stepped chutes. In their study, they reported comparatively larger integral turbulent scales with larger step heights. The smaller integral turbulent scales on the non-uniform stepped spillway might also be linked with scale effects for the smaller step height.

5 Free-surface observations

Transition and skimming flows down stepped spillways are characterised by unsteady wavy surface patterns in the non-aerated flow region at the upstream end (Fig. 2). In the region close to the inception point, free-surface instabilities and flapping of the free-surface was observed as previously reported (Chamani 2000, Chanson 2001). Downstream of the inception point of free-surface aeration, the air-water flow exhibited a more chaotic 'free-surface' appearance with strong splashing, ejection of water droplets (Chanson and Carosi 2007) and a strong mixing between air and water phases. A clear definition of the free-surface is impossible and a number of characteristic two-phase flow parameters are typically measured with the conductivity probe, e.g. characteristic depth Y_{90}, equivalent clear water flow depth d. A longitudinal distribution of these parameters was observed with a seesaw pattern of wave length of two step cavities, as reported in several studies (Boes 2000, Chanson and Toombes 2002, Felder and Chanson 2009). This seemed to be a characteristic of air-water skimming flows on stepped spillways. The finding suggested a wavy free-surface

pattern in the aerated flow region, similar to that as reported by Toombes and Chanson (2007). Herein a straight line of four acoustic displacement meters was used for non-intrusive measurements of the free-surface in both non-aerated and aerated flow regions on the non-uniform stepped spillway (Fig. 2b).

5.1. Free-surface profiles and fluctuations

Basic signal processing of the acoustic displacement signals yielded the mean free-surface elevation d_{50}, the 90% percentile of free-surface elevation d_{90} and the standard deviation of free-surface elevation d''. Typical dimensionless results are shown in Fig. 9 as functions of the dimensionless longitudinal distance along the stepped spillway x/d_c. Basically the flow depth decreased with increasing distance from the upstream end of the stepped spillway in the non-aerated flow region as the flow was accelerated. In the aerated flow region, the flow depth increased with distance, reflecting some flow bulking induced by free-surface aeration. The free-surface elevation data showed a wavy pattern with wave length of two step cavities, in particular visible in the non-aerated flow region (Fig. 9). In the aerated flow region, some data scatter was observed. The corresponding double-tip conductivity probe air-water flow data are included in Fig. 9: the mean free-surface elevations d_{50} were close to the equivalent clear water flow depth d while the characteristic flow depth Y_{90} was in agreement with d_{90} (Fig. 9). Bung (2011) reported slightly different results, namely a close agreement of the mean free-surface elevation d_{50} with a characteristic flow depth measured with a conductivity probe where $C = 0.80$. All present data exhibited a longitudinal seesaw pattern in both aerated and non-aerated flow regions, somehow similar to that observed in air-water flow experiments.

The present experimental data were compared with semi-empirical calculations of the developing boundary layer thickness and flow depth (Chanson 2001). The boundary layer thickness δ_{BL} was calculated at every location along the stepped spillway:

$$\frac{\delta_{BL}}{x} = 0.06106\ (\sin\theta)^{0.133} \left(\frac{\delta_{BL}}{h\cos\theta}\right)^{-0.17} \quad (7)$$

The theoretical estimate of flow depth d_B was calculated since the Bernoulli equation provides the ideal fluid velocity V_{max}:

$$V_{max} = \sqrt{2g(H_{max} - d_B\cos\theta)} \quad (8)$$

where H_{max} is the upstream total head and g is the gravity constant. In the ideal fluid flow region for $\delta_{BL} < y < d$, the real local velocity v may be approximated by Eq. (8) and experimental data suggested that the velocity distribution followed a power law (Chanson 2001):

$$\frac{v}{V_{max}} = \left(\frac{y}{\delta_{BL}}\right)^{1/N} \quad (9)$$

where the power law exponent was found as $1/N = 1/10$ for the present experiments. Following Eqs. (8) and (9), the flow depth d_B may be deduced by continuity:

$$d_B = \frac{q_w}{\sqrt{2g\,(H_{max} - d\ cos\,\theta)}} + \frac{\delta_{BL}}{N} \quad (10)$$

Equations (7) and (10) are shown in Fig. 9 for both aerated and non-aerated flows. For all experimental data, the calculations underestimated slightly the experimental data in both non-aerated and aerated flow regions. The differences were larger in the aerated flow region and tended to increase with increasing discharge. Note that Eq. (10) was not developed for the rapidly varying flow region downstream of the inception point, although it is shown in Fig. 9 for comparison only.

The free-surface fluctuations d'/d_c are shown in Fig. 10 as a function of of the longitudinal distance x/d_c. The standard deviation in the non-aerated flow region was relatively small and comparable for all flow rates. Downstream of the inception point of free-surface aeration, the free-surface fluctuations increased rapidly. Larger fluctuations in flow depths were observed for the smallest flow rate. This was linked with stronger droplet ejections for the smaller flow rate and with a shorter aerated flow region with increasing discharge. The large free-surface fluctuations in the aerated flow region highlighted the fluctuating nature of the air-water upper surface linked with the 'undefined' air-water free-surface, strong droplet ejections and wavy profiles (Chanson and Toombes 2007).

Spectral data analyses of the signals were performed in the aerated and non-aerated flow regions to identify the characteristic frequencies of free-surface fluctuations. The results indicated no dominant frequency. This might be linked with the limited data sampling capacity of the acoustic displacement meters of 100 Hz and a faster sensor response time might provide further insights.

5.2. Free-surface time scales and free-surface wave celerity

Auto-correlation analyses of acoustic displacement meter signals in the non-aerated and aerated regions were conducted to identify the characteristic time scales of free-surface fluctuations. Figure 11 illustrates the dimensional auto-correlation time scales in the non-aerated and aerated flow regions for three discharges, as well as the average and median data. The auto-correlation time scales in the non-aerated region were larger than in the aerated flow. In the aerated flow region, some data scatter was observed and the largest time scales were found for the smallest discharge. Overall, for all data sets, the average and median auto-correlation time scales were about 0.5 s at the upstream end of the non-aerated flow region. Further downstream in the non-aerated and aerated flow regions, the median values were within 0.05 to 0.2 s. The free-surface auto-correlation time scales was much larger than the auto- and cross-correlation time scales in the air-water flow region measured with phase-detection intrusive probes. The air-water flow auto- and cross-correlation time scales were one to two orders of magnitude smaller ($T_{xx} \approx T_{xy} \approx 0.001$-$0.01$ s). It is believed that the free-surface auto-correlation time scales were an indicator of large scale free-surface motion.

FELDER, S., and CHANSON, H. (2014). "Air–water Flows and Free-surface Profiles on a Non-uniform Stepped Chute." *Journal of Hydraulic Research*, IAHR, Vol. 52, No. 2, pp. 253-263 (DOI: 10.1080/00221686.2013.841780) (ISSN 0022-1686). {http://dx.doi.org/10.1080/00221686.2013.841780}

Cross-correlation analyses were performed between two simultaneously sampled acoustic displacement signals separated by a longitudinal distance x_j - x_i = 11 cm. The cross-correlation functions exhibited a clear peak, and the time for which the cross-correlation function was maximum T was used to calculate the free-surface wave celerity C_S of free-surface disturbances:

$$C_S = \frac{x_j - x_i}{T} \quad (9)$$

The free-surface wave celerity is a longitudinal measure of the free-surface velocity of the large scale wave structures in both non-aerated and aerated flows. Typical dimensionless celerity C_S/V_c distributions are illustrated in Fig. 12 for one discharge as functions of x/d_c. The celerity data showed an increase of values with increasing distance from the upstream end of the stepped spillway. Small scatter of the data was observed (Fig. 12). The free-surface wave celerity data were compared with the dimensionless air-water flow data measured with a double-tip conductivity probe, i.e. mean flow velocity U_w ($U_w = q_w/d$) and characteristic interfacial velocity V_{90}. The celerity data were close to the mean flow velocity U_w, but slightly smaller than the characteristic velocity V_{90} . The free-surface celerity increased slightly for larger flow rates, but the agreement with the corresponding air-water flow velocities remained unchanged. The present finding was significant because it indicated the effect of free-surface motions upon the air-water flow properties, as suggested by Toombes and Chanson (2007).

6 Conclusion

An experimental study was conducted on a non-uniform stepped spillway with regular alternation of step heights and the results were compared with the corresponding uniform stepped spillway for a same slope θ = 26.6º. The flow patterns showed small instabilities and larger droplet splashing on the non-uniform stepped configuration. Overall the flow regimes for the uniform and non-uniform stepped spillways were in close agreement, although larger instabilities were found on the non-uniform stepped chute. The air-water flow properties on both stepped configurations showed a good agreement between experimental data and theoretical solutions in terms of void fraction and interfacial velocity. Small differences were however observed in terms of bubble count rate, turbulence levels and integral turbulent scales. The comparative analyses between uniform and non-uniform stepped configurations suggested little effects of non-uniform steps upon the overall air-water flow structure. However, the appearance of larger flow instabilities and stronger variation of the air-water flow properties downstream of the large drop suggested that the uniform stepped spillway design might be the preferred design option.

On the non-uniform stepped spillway, a non-intrusive measurement technique was tested in both non-aerated and aerated flow regions. The free-surface profiles, free-surface fluctuations, free-surface time scales and the celerity of free-surface waves were documented. In the non-aerated flow region, the free-surface profiles were close to a theoretical prediction of the free-surface. In the aerated flow region, the acoustic displacement data showed a large scatter and the surface profile measurements agreed with

FELDER, S., and CHANSON, H. (2014). "Air–water Flows and Free-surface Profiles on a Non-uniform Stepped Chute." *Journal of Hydraulic Research*, IAHR, Vol. 52, No. 2, pp. 253-263 (DOI: 10.1080/00221686.2013.841780) (ISSN 0022-1686). {http://dx.doi.org/10.1080/00221686.2013.841780}

corresponding conductivity probe data. Despite large free-surface fluctuations in the aerated flow region, the experiments highlighted the successful use of acoustic displacement meters to record the free-surface properties in both non-aerated and aerated flow regions.

Acknowledgements

The authors thank Graham Illidge and Clive Booth for their technical assistance. The financial support through a UQ research scholarship is acknowledged.

Notation

C = void fraction

C_S = free-surface celerity (m/s)

C_{mean} = depth-averaged void fraction

D_o = dimensionless constant

d = equivalent clear water flow depth (m)

d' = free-surface fluctuations (m)

d_B = free-surface profile in empirical equation (m)

d_c = critical flow depth (m): $d_c = (q_w^2/g)^{1/3}$

d_{50} = mean free-surface elevation (m) measured with acoustic displacement meter

d_{90} = 90% percentile of free-surface elevation (m) measured with acoustic displacement meter

F = bubble count rate (Hz)

g = gravity acceleration constant (m/s^2)

H_{max} = maximum upstream head (m)

h = vertical step height (m)

K' = dimensionless integration constant

L_{xz} = transverse integral turbulent length scale (m)

N = power law exponent

q_w = discharge per unit width (m^2/s)

R = Reynolds number in terms of the hydraulic diameter

$(R_{xz})_{max}$ = maximum transverse cross-correlation coefficient

T = time lag (s)

FELDER, S., and CHANSON, H. (2014). "Air–water Flows and Free-surface Profiles on a Non-uniform Stepped Chute." *Journal of Hydraulic Research*, IAHR, Vol. 52, No. 2, pp. 253-263 (DOI: 10.1080/00221686.2013.841780) (ISSN 0022-1686). {http://dx.doi.org/10.1080/00221686.2013.841780}

Tu = turbulence intensity

T_{int} = transverse integral turbulent time scale (s)

T_{xx} = auto-correlation time scale (s)

T_{xy} = streamwise cross-correlation time scale (s)

T_{xz} = transverse cross-correlation time scale (s)

U_w = mean flow velocity (m/s)

V = interfacial velocity (m/s)

V_c = critical flow velocity (m/s): $V_c = (g\ d_c)^{0.5}$

V_{max} = maximum interfacial velocity (m/s)

V_{90} = characteristic interfacial velocity (m/s)

v = local velocity (m/s)

W = channel width (m)

x = distance along the channel bottom (m)

Y_{90} = characteristic flow depth (m)

y = distance normal to the invert (m)

z = transverse distance from channel centreline (m)

Δx = streamwise separation distance between sensors (m)

Δz = transverse separation distance between sensors (m)

δ_{BL} = boundary layer thickness (m)

θ = channel slope

$Ø$ = sensor diameter (m)

References

Amador, A., Sánchez-Juny, M., Dolz, J. (2006). Characterization of the nonaerated flow region in a stepped Spillway by PIV. *J. Fluids Eng*. 128(6), 1266-1273.

Boes, R.M. (2000). Zweiphasenströmung und Energieumsetzung an Grosskaskaden. (Two-phase flow and energy dissipation on cascades.) *Ph.D. Thesis*, VAW-ETH, Zürich, Switzerland (in German). (also Mitteilungen der Versuchsanstalt für Wasserbau, Hydrologie and Glaziologie, ETH-Zürich, Switzerland, No. 166).

FELDER, S., and CHANSON, H. (2014). "Air–water Flows and Free-surface Profiles on a Non-uniform Stepped Chute." *Journal of Hydraulic Research*, IAHR, Vol. 52, No. 2, pp. 253-263 (DOI: 10.1080/00221686.2013.841780) (ISSN 0022-1686). {http://dx.doi.org/10.1080/00221686.2013.841780}

Boes, R.M., Hager, W.H. (2003). Hydraulic design of stepped spillways. *J. Hydraulic Eng.* 129(9), 671–679.

Bung, D.B. (2011). Non-intrusive measuring of air-water flow properties in self-aerated stepped spillway flow. Proc. *34th IAHR 2011 Congress*, Brisbane, Australia, 2380-2387.

Bung, D.B. (2013). Non-intrusive detection of air–water surface roughness in self-aerated chute flows. *J. Hydraulic Res.* 51(3), 322-329.

Chamani, M.R. (2000). Air Inception in Skimming Flow Regime over Stepped Spillways. *Proc. Intl Workshop on Hydraulics of Stepped Spillways*, Zürich, Switzerland, H.E. Minor & W.H. Hager Editors, Balkema Publ., pp. 61-67.

Chanson, H. (2001). *The hydraulics of stepped chutes and spillways.* Balkema, Lisse, The Netherlands, 418 pages.

Chanson, H., Carosi, G. (2007). Turbulent time and length scale measurements in high-velocity open channel flows. *Exp. Fluids* 42(3), 385-401.

Chanson, H., Toombes, L. (2002). Air-water flows down stepped chutes: Turbulence and flow structure observations. *Intl. J. Multiphase Flow* 28(11), 1737-1761.

Chanson, H., Toombes, L. (2004). Hydraulics of stepped chutes: The transition flow. *J. Hydraulic Res*. 42(1), 43-54.

Felder, S. (2013). Air-water flow properties on stepped spillways for embankment dams: Aeration, energy dissipation and turbulence on uniform, non-uniform and pooled stepped chutes. *Ph.D. thesis*, School of Civil Engineering, University of Queensland, Australia.

Felder, S., Chanson, H. (2009). Turbulence, dynamic similarity and scale effects in high-velocity free-surface flows above a stepped chute. *Exp. Fluids* 47(1), 1-18.

Felder, S., Chanson, H. (2011). Energy dissipation down a stepped spillway with non-uniform step heights. *J. Hydraulic Eng.* 137(11), 1543-1548.

Gonzalez, C.A., Chanson, H. (2004). Interactions between cavity flow and main stream skimming flows: an experimental study. *Can. J. Civil Eng.* 31(1), 33-44.

Gonzalez, C.A., Chanson, H. (2007a). Hydraulic design of stepped spillways and down-stream energy dissipators for embankment dams. *Dam Engineering* 17(4), 223-244.

Gonzalez, C.A., Chanson, H. (2007b). Experimental measurements of velocity and pressure distribution on a large broad-crested weir. *Flow Meas. Instrum.* 18, 107-113.

Hunt S.L., Kadavy, K.C. (2010). Energy dissipation on flat-sloped stepped spillways: Part 1. Upstream of the inception point. *Trans. ASABE* 53(1), 103-109.

FELDER, S., and CHANSON, H. (2014). "Air–water Flows and Free-surface Profiles on a Non-uniform Stepped Chute." *Journal of Hydraulic Research*, IAHR, Vol. 52, No. 2, pp. 253-263 (DOI: 10.1080/00221686.2013.841780) (ISSN 0022-1686). {http://dx.doi.org/10.1080/00221686.2013.841780}

Matos, J. (2000). Hydraulic design of stepped spillways over RCC dams. Intl Workshop on *Hydraulics of Stepped Spillways*, Zürich, Switzerland, 187-194.

Meireles, I., Matos, J. (2009). Skimming flow in the nonaerated region of stepped spillways over embankment dams. *J. Hydraulic Eng.* 135(8), 685-689.

Murzyn, F., Chanson, H. (2009). Free-surface fluctuations in hydraulic jumps: Experimental observations. *Exp. Therm. Fluid Sci.* 33(7), 1055-1064.

Ohtsu, I., Yasuda, Y., Takahashi, M. (2004). Flow characteristics of skimming flows in stepped channels. *J. Hydraulic Eng.* 130(9), 860-869.

Rajaratnam, N. (1990). Skimming flow in stepped spillways. *J. Hydraulic Eng.* 116(4), 587-591.

Stephenson, D. (1988). Stepped energy dissipators. Proc. *International Symposium on Hydraulics for High Dams*, Beijing, China, 1228-1235.

Toombes, L. (2002). Experimental study of air-water flow properties on low-gradient stepped cascades. *Ph.D. Thesis*, Dept. of Civil Engineering, University of Queensland, Australia.

Toombes, L., Chanson, H. (2007). Surface waves and roughness in self-aerated supercritical flow. *Environ. Fluid Mech.* 5(3), 259-270.

Toombes, L., Chanson, H. (2008). Flow patterns in nappe flow regime down low gradient stepped chutes. *J. Hydraulic Res*. 46(1), 4-14

Table 1 Experimental flow conditions for stepped spillway experiments with conductivity probes and acoustic displacement meters in the present study

Spillway configuration	Instrumentation	d_c/h	q_w (m^2/s)	R	U_w (m/s)	V_{90} (m/s)
Non-uniform	2-tip conductivity probe	0.69-1.74(*)	0.056-0.227	2.2×10^5-9.0×10^5	2.1-3.4	2.4-4.4
	Array of two 1-tip conductivity probes	1.11(*)	0.116	4.6×10^5	≈ 2.6	N/A
	Four acoustic displacement meters	0.83-1.61(*)	0.075-0.202	3.0×10^5-8.0×10^5	N/A	N/A
Uniform	2-tip conductivity probe	0.69-1.74	0.056-0.227	2.2×10^5-9.0×10^5	2.2-3.1	2.4-4.2
	Array of two 1-tip conductivity probes	1.11	0.116	4.6×10^5	≈ 2.5	N/A

Notes: (*) calculated for h = 10 cm; N/A – velocity property not measured

FELDER, S., and CHANSON, H. (2014). "Air–water Flows and Free-surface Profiles on a Non-uniform Stepped Chute." *Journal of Hydraulic Research*, IAHR, Vol. 52, No. 2, pp. 253-263 (DOI: 10.1080/00221686.2013.841780) (ISSN 0022-1686). {http://dx.doi.org/10.1080/00221686.2013.841780}

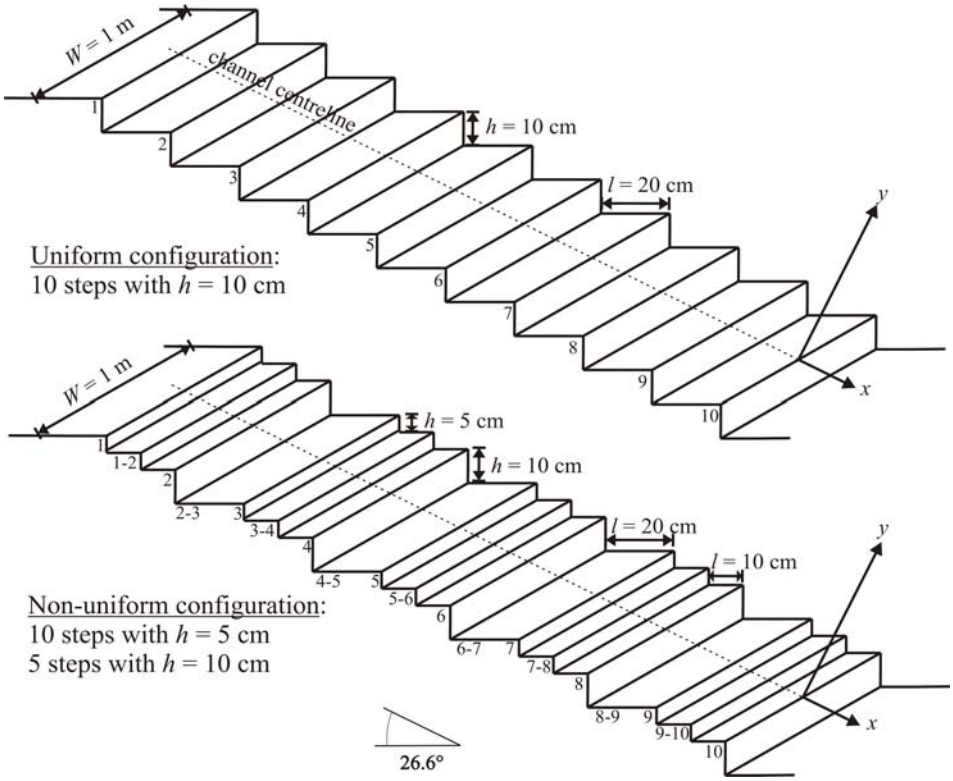

Figure 1 Stepped spillway configurations with uniform and non-uniform steps; experimental setup and definition of step numbering and measurement positions at and between step edges

FELDER, S., and CHANSON, H. (2014). "Air–water Flows and Free-surface Profiles on a Non-uniform Stepped Chute." *Journal of Hydraulic Research*, IAHR, Vol. 52, No. 2, pp. 253-263 (DOI: 10.1080/00221686.2013.841780) (ISSN 0022-1686). {http://dx.doi.org/10.1080/00221686.2013.841780}

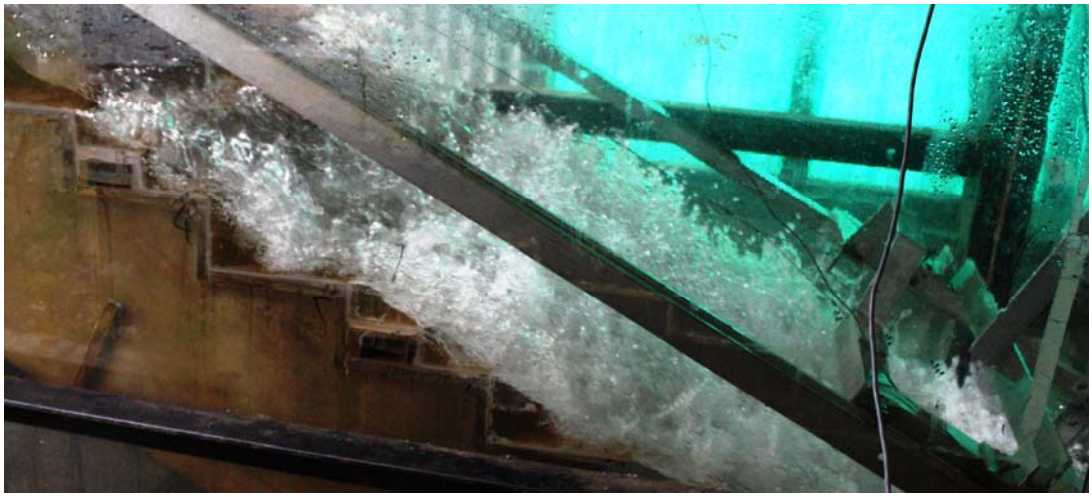

(a) Transition flow regime: $d_c/h = 0.78$, $q_w = 0.069$ m^2/s, R = 2.7×10^5; note the trolley for the double-tip conductivity probe in the right bottom corner

(b) Free-surface waves and fluctuations in the skimming flow regime: $d_c/h = 1.46$, $q_w = 0.175$ m^2/s, R = 6.9×10^5; wooden support with the acoustic displacement meters above the air-water flows

Figure 2 Air-water flow patterns on the non-uniform stepped spillway

FELDER, S., and CHANSON, H. (2014). "Air–water Flows and Free-surface Profiles on a Non-uniform Stepped Chute." *Journal of Hydraulic Research*, IAHR, Vol. 52, No. 2, pp. 253-263 (DOI: 10.1080/00221686.2013.841780) (ISSN 0022-1686). {http://dx.doi.org/10.1080/00221686.2013.841780}

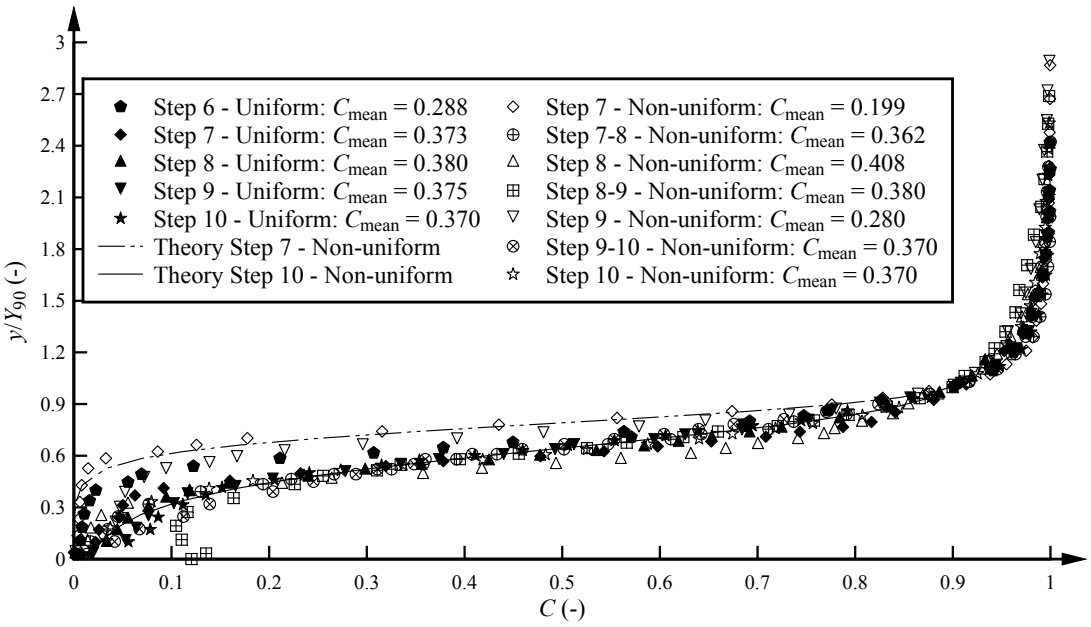

Figure 3 Void fraction distributions on the stepped spillways with uniform and non-uniform steps; comparison with advective diffusion equation (Eq. (3)); d_c/h = 1.11, q_w = 0.116 m^2/s, R = 4.6 × 10^5

FELDER, S., and CHANSON, H. (2014). "Air–water Flows and Free-surface Profiles on a Non-uniform Stepped Chute." *Journal of Hydraulic Research*, IAHR, Vol. 52, No. 2, pp. 253-263 (DOI: 10.1080/00221686.2013.841780) (ISSN 0022-1686). {http://dx.doi.org/10.1080/00221686.2013.841780}

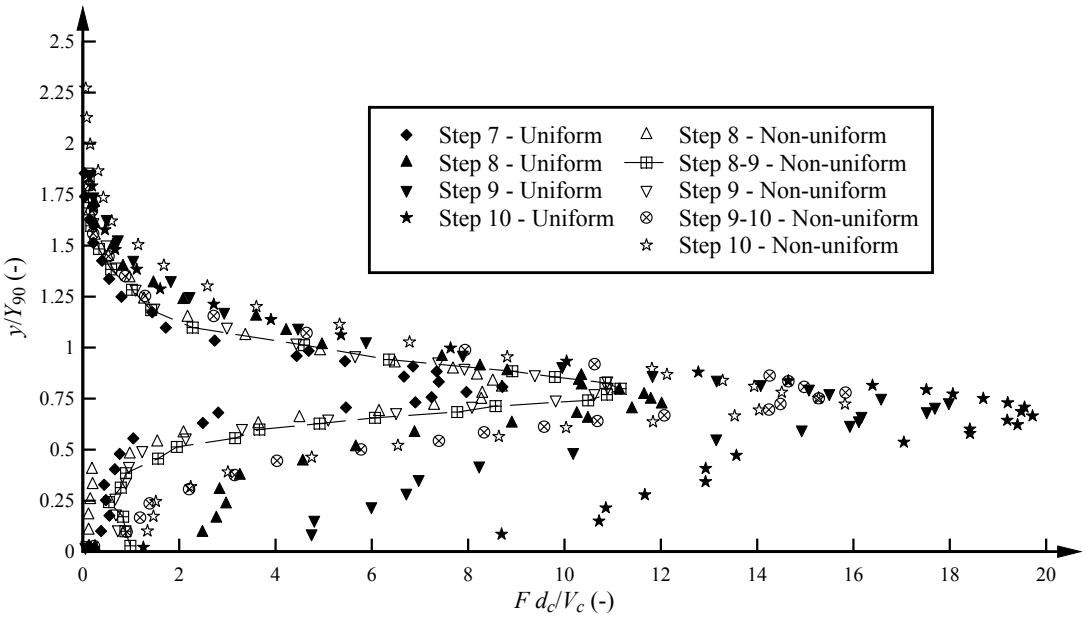

Figure 4 Bubble count rate distributions on the stepped spillways with uniform and non-uniform steps; d_c/h = 1.38, q_w = 0.161 m^2/s, R = 6.4 × 10^5

FELDER, S., and CHANSON, H. (2014). "Air–water Flows and Free-surface Profiles on a Non-uniform Stepped Chute." *Journal of Hydraulic Research*, IAHR, Vol. 52, No. 2, pp. 253-263 (DOI: 10.1080/00221686.2013.841780) (ISSN 0022-1686). {http://dx.doi.org/10.1080/00221686.2013.841780}

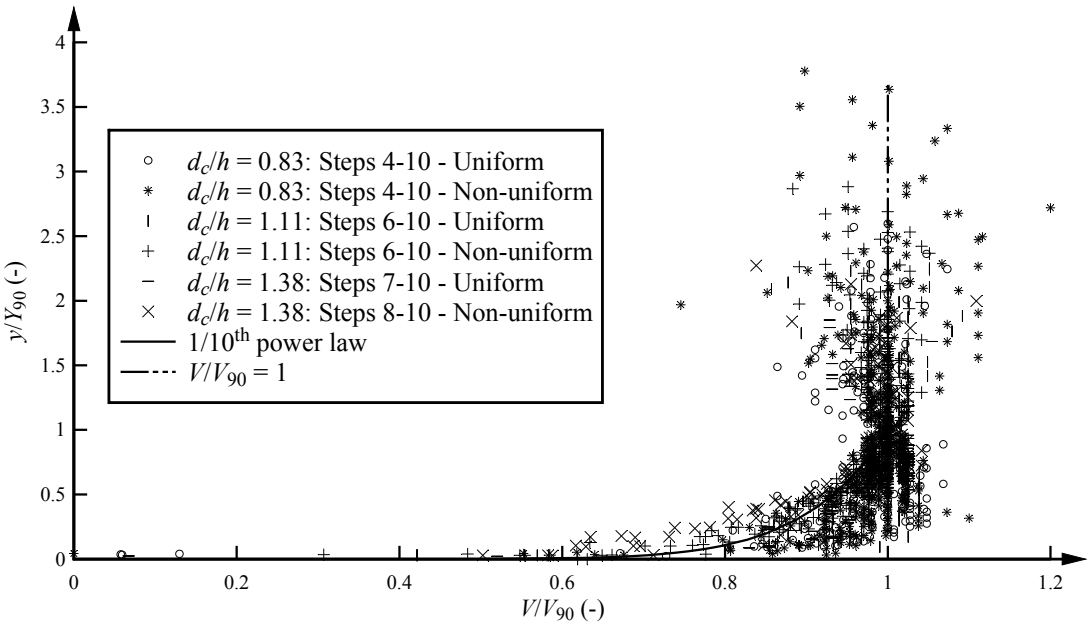

Figure 5 Dimensionless interfacial velocity distributions on the stepped spillways with uniform and non-uniform steps; comparison with power law and uniform profile (Eqs. (5) and (6))

FELDER, S., and CHANSON, H. (2014). "Air–water Flows and Free-surface Profiles on a Non-uniform Stepped Chute." *Journal of Hydraulic Research*, IAHR, Vol. 52, No. 2, pp. 253-263 (DOI: 10.1080/00221686.2013.841780) (ISSN 0022-1686). {http://dx.doi.org/10.1080/00221686.2013.841780}

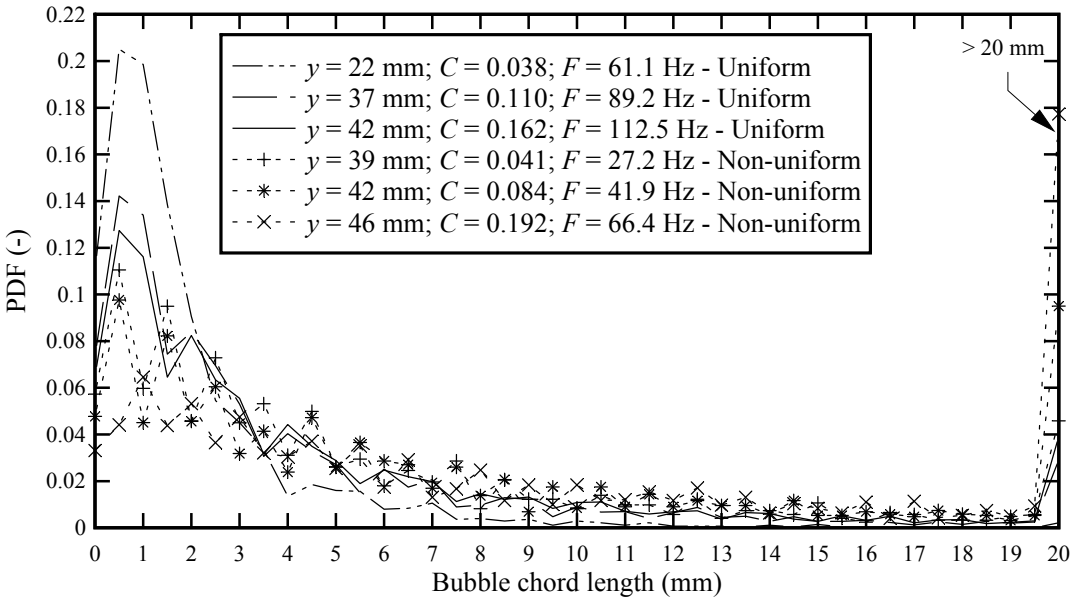

(a) Air bubble chord length: d_c/h = 1.38, q_w = 0.161 m^2/s, R = 6.4 × 10^5, Step 9

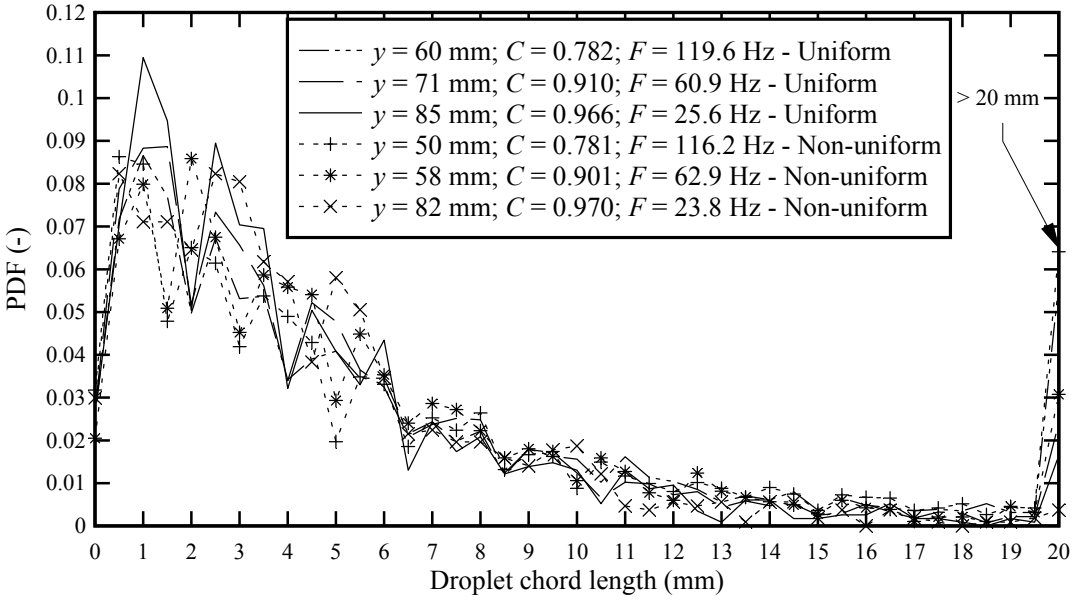

(b) Water droplet chord length: d_c/h = 1.11, q_w = 0.116 m^2/s, R = 4.6 × 10^5, Step 9

Figure 6 Chord size probability distributions on the stepped spillways with uniform and non-uniform steps

FELDER, S., and CHANSON, H. (2014). "Air–water Flows and Free-surface Profiles on a Non-uniform Stepped Chute." *Journal of Hydraulic Research*, IAHR, Vol. 52, No. 2, pp. 253-263 (DOI: 10.1080/00221686.2013.841780) (ISSN 0022-1686). {http://dx.doi.org/10.1080/00221686.2013.841780}

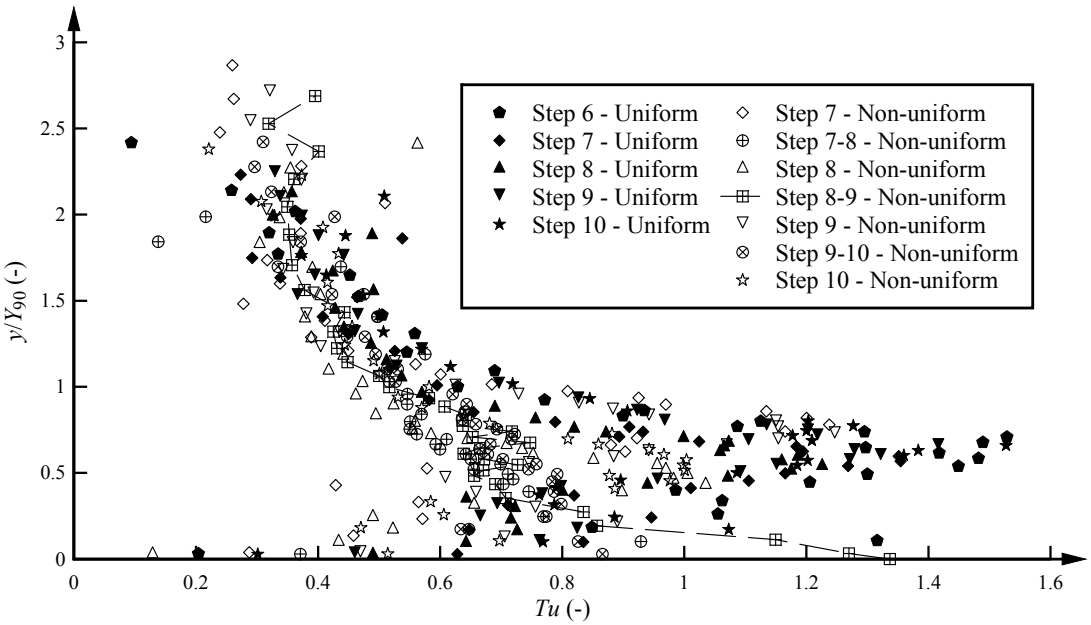

Figure 7 Turbulence intensity distributions on the stepped spillways with uniform and non-uniform steps; $d_c/h = 1.11$, $q_w = 0.116$ m^2/s, R = 4.6×10^5

FELDER, S., and CHANSON, H. (2014). "Air–water Flows and Free-surface Profiles on a Non-uniform Stepped Chute." *Journal of Hydraulic Research*, IAHR, Vol. 52, No. 2, pp. 253-263 (DOI: 10.1080/00221686.2013.841780) (ISSN 0022-1686). {http://dx.doi.org/10.1080/00221686.2013.841780}

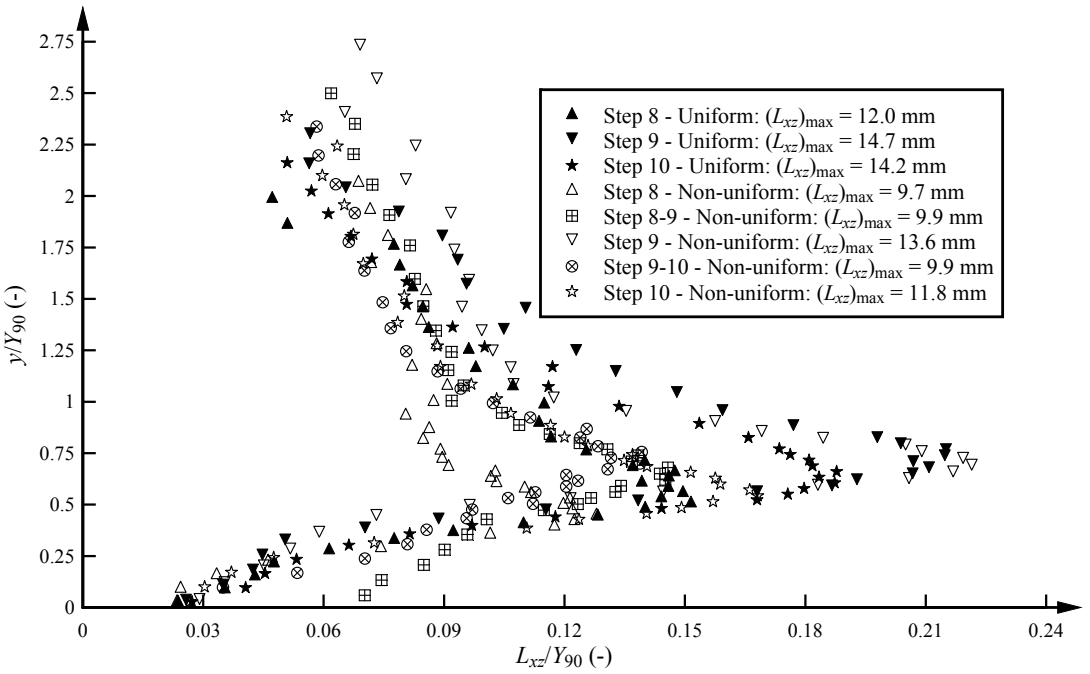

(a) Integral turbulent length scale

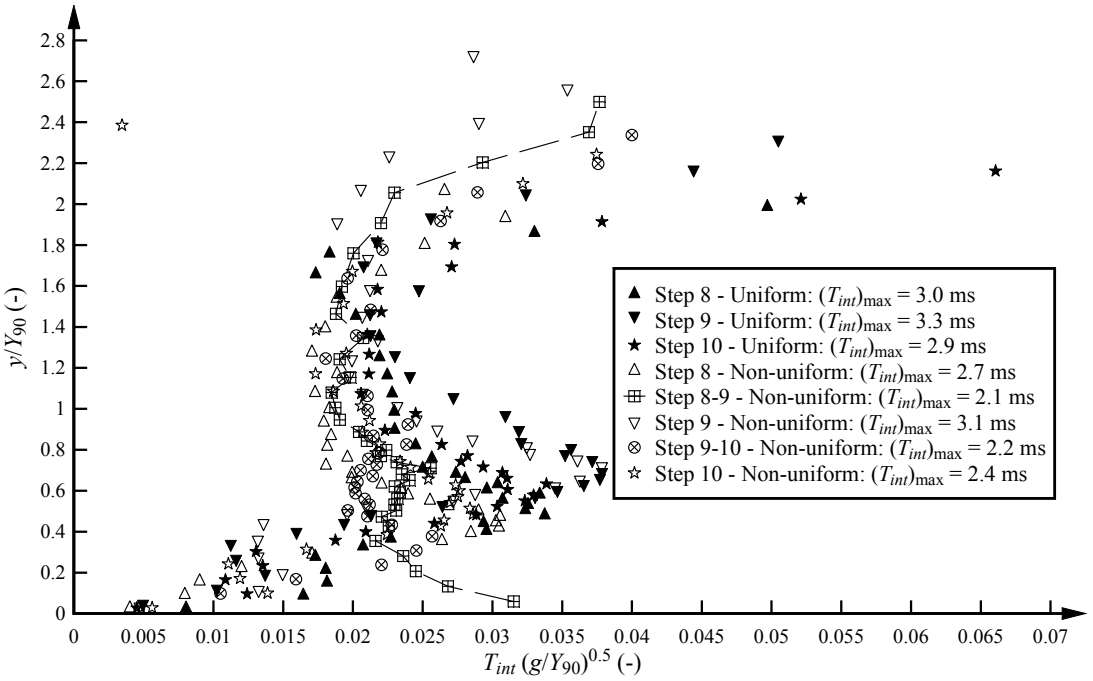

(b) Integral turbulent time scale

Figure 8 Dimensionless integral turbulent length and time scale distributions on the stepped spillways with uniform and non-uniform steps; d_c/h = 1.11, q_w = 0.116 m^2/s, R = 4.6 × 10^5

FELDER, S., and CHANSON, H. (2014). "Air–water Flows and Free-surface Profiles on a Non-uniform Stepped Chute." *Journal of Hydraulic Research*, IAHR, Vol. 52, No. 2, pp. 253-263 (DOI: 10.1080/00221686.2013.841780) (ISSN 0022-1686). {http://dx.doi.org/10.1080/00221686.2013.841780}

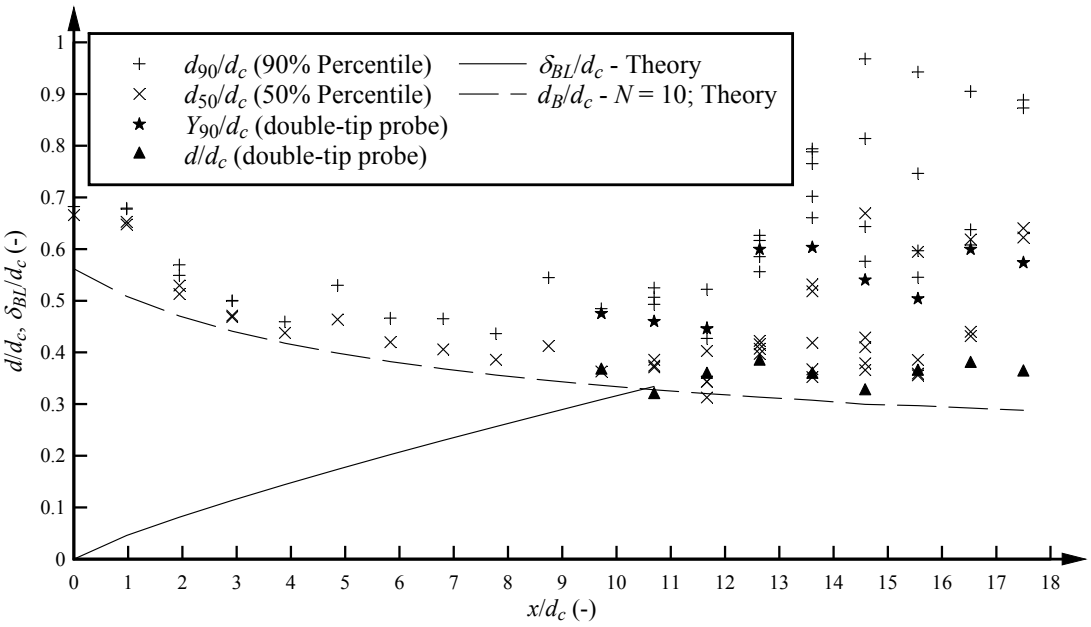

Figure 9 Free-surface profiles on the non-uniform stepped spillway; comparison with air-water flow data and theory of boundary layer development and flow depth (Eqs. (7) and (10)); d_c/h = 1.11, q_w = 0.116 m^2/s, R = 4.6 × 10^5

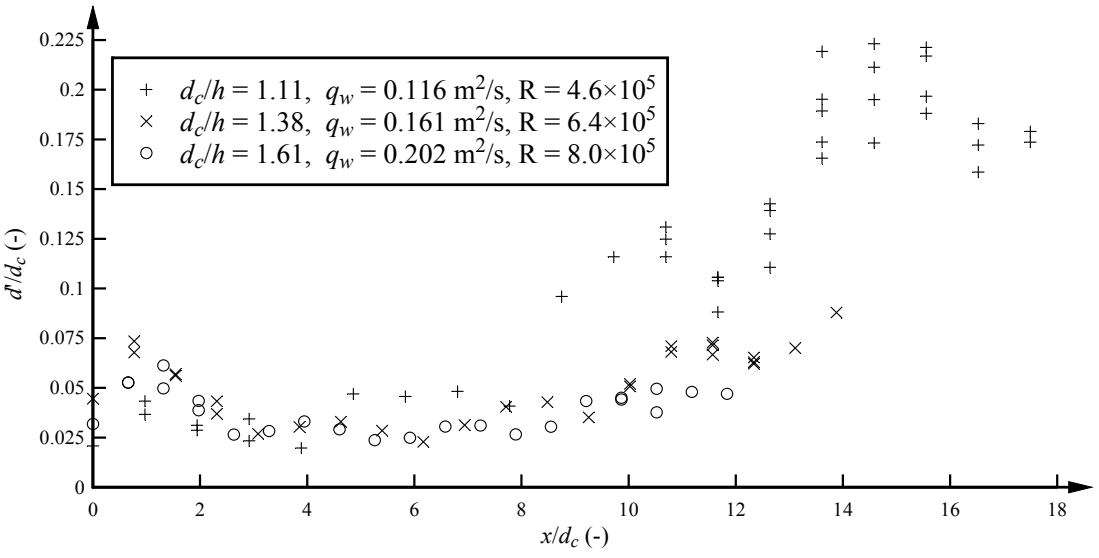

Figure 10 Standard deviation of free-surface profiles on the non-uniform stepped spillway

FELDER, S., and CHANSON, H. (2014). "Air–water Flows and Free-surface Profiles on a Non-uniform Stepped Chute." *Journal of Hydraulic Research*, IAHR, Vol. 52, No. 2, pp. 253-263 (DOI: 10.1080/00221686.2013.841780) (ISSN 0022-1686). {http://dx.doi.org/10.1080/00221686.2013.841780}

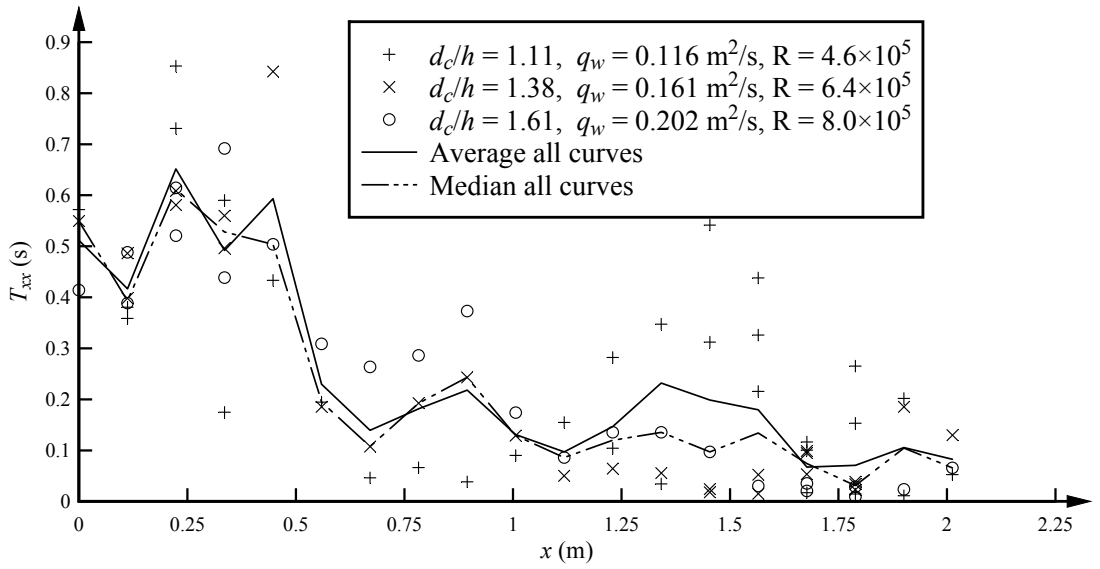

Figure 11 Auto-correlation time scales of the free-surface on the non-uniform stepped spillway

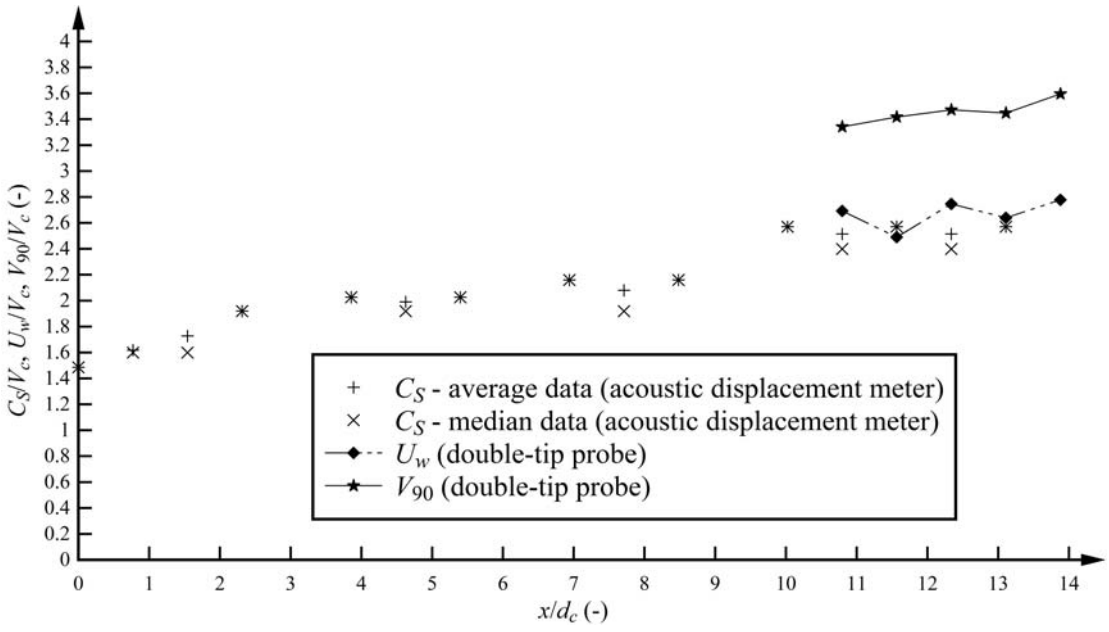

Figure 12 Free-surface wave celerity on the non-uniform stepped spillway; comparison with air-water flow data; d_c/h = 1.38, q_w = 0.161 m^2/s, R = 6.4 × 10^5